remote sensing

MDPI

Article

Remote Sensing-Supported Flood Forecasting of Urbanized Watersheds—A Case Study in Southern China

Yu Gu, Yangbo Chen *, Huaizhang Sun and Jun Liu

School of Geography and Planning, Sun Yat-sen University, Guangzhou 510275, China
* Correspondence: eescyb@mail.sysu.edu.cn; Tel.: +86-20-8411-4269

Abstract: Urbanization has significant impacts on watershed hydrology, but previous studies have been confirmatory and not comprehensive; in particular, few studies have addressed the impact of urbanization on flooding in highly urbanized watersheds. In this study, this effect is studied in Chebei Creek, a highly urbanized watershed in the Pearl River Delta, southern China. Landsat satellite images acquired in 2015 were used to estimate land use and cover changes using the Decision Tree (DT) C4.5 classification algorithm, while the Liuxihe model, a physically based distributed hydrological model (PBDHM), is employed to simulate watershed flooding and hydrological processes. For areas with high degrees of urbanization, the duration of the flood peak is only 1 h, and the flood water level shows steep rises and falls. These characteristics increase the difficulty of flood modeling and forecasting in urbanized areas. At present, hydrological research in urbanized watersheds generally focuses on the quantitative simulation of runoff from urban areas to the watershed, flood flows, peak flood flow, and runoff depth. Few studies have involved real-time flood forecasting in urbanized watersheds. To achieve real-time flood forecasting in urbanized watersheds, PBDHMs and refined underlying surface data based on remote sensing technology are necessary. The Liuxihe model is a PBDHM that can meet the accuracy requirements of inflow flood forecasting for reservoir flood control operations. The accuracies of the two flood forecasting methods used in this study were 83.95% and 97.06%, showing the excellent performance of the Liuxihe model for the real-time flood forecasting of urbanized rivers such as the Chebei Creek watershed.

Keywords: urbanization; Liuxihe model; land use/cover changes; flood forecasting; remote sensing

Citation: Gu, Y.; Chen, Y.; Sun, H.; Liu, J. Remote Sensing-Supported Flood Forecasting of Urbanized Watersheds—A Case Study in Southern China. *Remote Sens.* **2022**, *14*, 6129. https://doi.org/10.3390/rs14236129

Academic Editors: Pingping Luo, Xindong Wei, Kanhua Yu, Bin Guo, Joshua Viers and Deodato Tapete

Received: 18 October 2022
Accepted: 29 November 2022
Published: 3 December 2022

1. Introduction

The world has experienced massive urbanization over the last century, with the global urban population surpassing the rural population for the first time in 2009 [1]. Developed countries began urbanizing earlier, and the process of urbanization has not yet ended [2]. In contrast, developing countries began urbanizing later, and urbanization has progressed more rapidly [3]. While urbanization involves the rapid development of a society, economy, and population, it also has significant impacts on watershed hydrological processes in urbanized areas [4–7]. Urbanization changes the hydrological processes of the watershed as well as the land use/cover (LUC) type of the watershed and generally transforms permeable surfaces into impervious surfaces [8–10]. Such changes hamper accurate flood forecasting in the basin, and this difficulty requires addressing.

With the development of hydrological models, scholars have begun to use hydrological modeling methods to study the hydrological effects of urbanization [11–13]. Hydrological modeling provides a novel method for studying the hydrological effects of urbanization in areas with no or few data available [14,15]. Hydrological models are key tools for real-time flood forecasting in urbanized watersheds. The first generation of watershed hydrological models employed lumped models [16,17], such as NAM [18], HBV [19], SCS [20,21], and HEC-HMS [22,23]. Since its development, the SWAT semi-distributed model has been widely used in scientific research, as it uses the surface cover type to

determine model parameters [24–26]. Lumped models calibrate the model parameters based on observed hydrological data, but because the characteristics of the underlying surface of the watershed are constantly changing in the process of urbanization, model parameters obtained from past observations do not reflect the hydrological characteristics of the watershed after urbanization [27,28].

With the introduction and continuous improvement of satellite remote sensing [29], geographic information systems [30], and supercomputing technologies, the physically based distributed hydrological model (PBDHM) has developed rapidly. The key technologies of PBDHM include hydrological modeling and the estimation of the characteristics of the underlying basin surface from satellite remote sensing data. Synthetic aperture radar (SAR) sensing has become increasingly important in various fields and is widely used to monitor natural hazards, land cover classification, change detection, maritime traffic control, and surface parameter inversion [31,32]. In addition, remote sensing images from the Landsat satellite are an important data source for the quantitative estimation of large-scale and long-term LUC changes [33–35]. Landsat satellite imagery is archived back to 1978 and has a spatial resolution of up to 30 m $\times$ 30 m, enabling the mapping of LUC changes in watersheds in developing regions that began to urbanize significantly after 1978. LUC estimation from satellite remote sensing data is mainly conducted using automatic classification algorithms [33]. Commonly used automatic classification algorithms include the decision tree [36], artificial neural network [37], support vector machine (SVM) [38], expectation–maximization-based learning [39], and affinity propagation clustering algorithms [40]. Applicability to LUC estimation differs among algorithms. To minimize the impact of the complexity of ground objects and combine the advantages of various algorithms, research on multi-classifier ensemble classification algorithms has become common in recent years [41,42]. To improve the accuracy of the classification results, LUC estimates from automatic classification algorithms often require manual post-processing to refine the underlying surface data.

PBDHM divides the study area into fine-scale grid cells [43], allowing the model to fully consider the physical properties of the watershed as well as the spatial and temporal heterogeneity of rainfall. Representative distributed hydrological models include SHE [14,44,45], VIC [15,46], DHSVM [47], WetSpa [48,49], GBHM [50], WEP [51], WEHY [52], and the Liuxihe model [53]. Compared to lumped models, PBDHMs have more potential for finely and accurately modeling and forecasting hydrological processes in watersheds [54]. PBDHM derives the model parameters at the physical level according to the topographic properties of the watershed, rather than calibrating the model parameters with the observed hydrological data. This process has obvious advantages for the hydrological simulation of urbanized watersheds affected by urbanization, where the characteristics of the underlying watershed surface are constantly changing [55].

To date, researchers around the world have conducted studies on the hydrological modeling of urbanization. Their results have focused on the increases in the runoff [44,56], runoff coefficient [20,57], flood flows [58], peak flow [59], and average annual runoff depth [60,61] of basins after urbanization. Getachew and Melesse [62] used hydrological simulations to determine that the average wet-season monthly runoff and dry-season monthly runoff in Ethiopia's Angereb watershed changed from 1985 to 2011, with increases of 39% and 46%, respectively. Miller et al. [25] found that, between 1960 and 2010, the urbanization levels of two small watersheds in the UK increased from 11% to 44%, while the flood confluence time was shortened by half, and the peak flow increased by 400%. Recent hydrological research in urbanized watersheds has focused mostly on water quality [63,64], the aquatic environment [65,66], the quantitative simulation of runoff from urban areas to the watershed, flood flows, peak flow, and runoff depth. Few studies have examined the utility of hydrological models for flood forecasting in urbanized watersheds.

To explore the applicability and stability of the PBDHM model for forecasting floods in the urbanized watershed, the Liuxihe model is employed in this study, and the Chebei Creek watershed in Guangdong Province is used as the research area. This study has

two objectives: to use the Liuxihe model to construct a flood forecasting model for the Chebei Creek watershed, along with the verification of the model in the real-time flood forecasting of the urbanized watershed for the first time; and to analyze the flood forecasting accuracy of the Liuxihe model in the Chebei Creek watershed, which is expected to provide a scientific basis for the application of the proposed flood forecasting scheme to other urbanized watersheds.

2. Methods and Materials

2.1. Liuxihe Model

The Liuxihe model is employed as the hydrological model for flood simulation in this study. The Liuxihe model is a physically based distributed watershed hydrological model proposed for watershed flood forecasting and has been applied in several watershed flood forecasting studies [53,67–69]. The model divides the watershed into grid cells using a digital elevation model, calculates evapotranspiration and production at the cell scale, and then converges cell-by-cell to the outlet of the basin through a confluence network. The confluence is divided into slope confluences and river confluences using the kinematical wave approximation and diffusive wave approximation methods, respectively, for calculation [53]. Each grid cell has unique terrain properties, including elevation, soil type, and LUC type, allowing the model to describe the inhomogeneity of terrain properties across the watershed. The Liuxihe model is a fully distributed hydrological model and thus has the ability to simulate flood hydrological processes. This model categorizes model parameters into four types, including climate-, topography-, vegetation-, and soil-based parameters, and each type is physically related to only one terrain property and is derived physically from that terrain property. For this reason, it can be used in watersheds with no river discharge observations. The model includes a parameter optimization method based on the particle swarm optimization (PSO) algorithm [69], which allows parameters to be optimized using reliable observation data, even if few data are available. The framework of the Liuxihe model is illustrated in Figure 1.

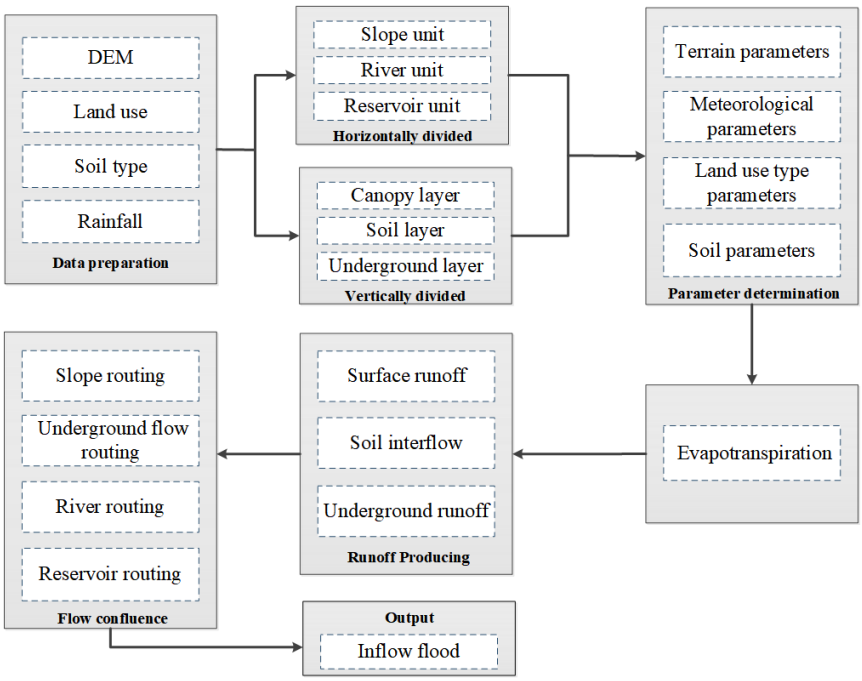

Figure 1. Framework of the Liuxihe model.

2.2. Chebei Creek Watershed

Chebei Creek was selected as the study watershed and is a highly urbanized watershed draining to the Guangzhou city center. The watershed has a drainage area of 65 km^2 with

a length of 20.4 km. The upper reaches of the basin are dominated by mountains and hills, while the lower reaches are dominated by plains. The terrain gradually flattens from north to south, and the elevation range varies greatly, ranging from 2.0 m to 390.0 m. As floodwaters will be directly discharged into the city center through the Chebei Creek, the flooding of Chebei Creek is a serious threat to the security of Guangzhou City, the capital of Guangdong Province and a major center of southern China. Figure 2 shows the location of the creek.

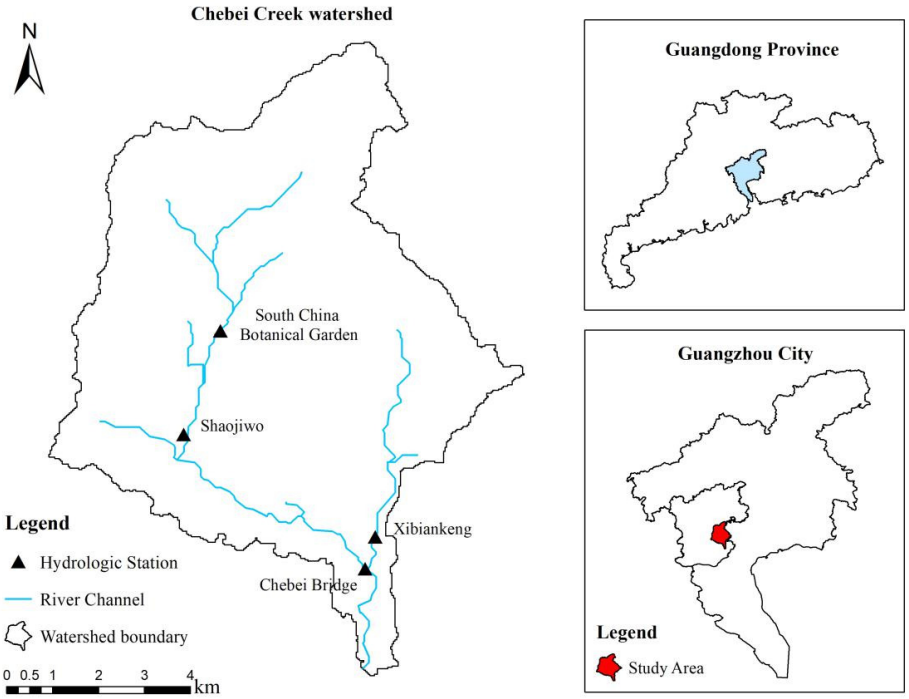

Figure 2. Location and map of the Chebei Creek watershed.

Chebei Creek is in the subtropical oceanic monsoon area, with an average annual temperature of 22.3 °C and an average annual rainfall of 1720 mm. Flooding occurs frequently due to heavy precipitation during the summer monsoon season [70]. Rapid urbanization over the past three decades has sharply altered its LUC, and urbanized land now dominates the watershed. Flooding has been enhanced during this rapid urbanization process, and increasing flood damage has been observed in recent years [71–74].

2.3. Terrain Property Data

2.3.1. Digital Elevation Model Data

The terrain property data required for the Liuxihe model setup and parameter derivation include the digital elevation model (DEM), soil map, and LUC map, with DEM data forming the basis of the Liuxihe model structure. The quality of DEM data directly affects important geographical parameters such as the slope of the watershed, the area of the watershed, and the length of the river. DEM data are also the most important data type for constructing the Liuxihe model.

Currently, many DEM datasets are available to download for free worldwide, including ASTER GDEM, AW3D30, NASADEM, and SRTM. However, Chebei Creek has an urbanized watershed with a small area. To improve flood prediction accuracy in this urbanized watershed, more refined DEM data are needed. A 1:10,000 vector topographic map of Guangzhou City produced recently was used to produce a DEM with a spatial resolution of 30 m, as shown in Figure 3. The average, highest, and lowest elevations of Chebei Creek are 66.13 m, 390.08 m, and 2.10 m, respectively.

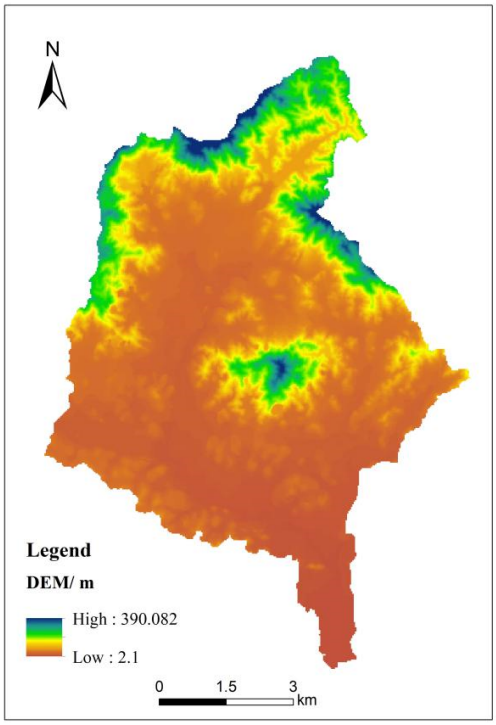

Figure 3. DEM of the Chebei Creek watershed produced using a 1:10,000 vector topographic map of Guangzhou City.

2.3.2. Land Use/Cover Data

Archived Landsat satellite images were downloaded from the United States Geological Survey (USGS) website (http://glovis.usgs.gov/ (accessed on 27 March 2021)) for estimating LUC changes in the study watershed. To update the underlying surface data of the Chebei Creek watershed, we estimated the LUC types of this watershed in 2015 using Landsat satellite images.

The decision tree (DT) C4.5 algorithm was employed in this study to classify the LUC types of the study watershed [36]. Six LUC types, including urban land (impervious surface), water body, forestry land, farm land, grass land, and bare land, were used in the classification. The LUCs automatically estimated by DT C4.5 were corrected through visual interpretation to increase the classification accuracy. The LUC estimated automatically by DT C4.5 was designated as the automated LUC, while that corrected by visual interpretation was designated as the corrected LUC (Figure 4). The average accuracy of the automated LUC classification was 88.12%, with an average Kappa coefficient of 0.868.

2.3.3. Soil Type Data

Soil types of the study watershed were extracted from the Food and Agriculture Organization of the United Nations (FAO) world soil map dataset (www.isric.org (accessed on 25 March 2021)) at a spatial resolution of 1 km and were rescaled to a spatial resolution of 30 m, as shown in Figure 5. One virtual soil type, urban soil, was added to facilitate the hydrological modeling of impervious surfaces; these soils could be any real soil type with urban land cover. The FAO soil map is not very recent, and urban land is not included; therefore, this map requires updates with LUC estimates. In 1987, three soil types were included in the FAO dataset for Chebei Creek, and the updated soil map has four soil types, including urban land (6.02%), Acric Ferralsol (67.08%), Eutric Cambisol (10.92%), and Ferric Acrisol (15.98%). In 2015, four were still present but their percentages had changed sharply to urban (52.71%), Acric Ferralsol (35.46%), Eutric Cambisol (4.02%), and Ferric Acrisol (7.81%), with urban land and Acric Ferralsol becoming the major types.

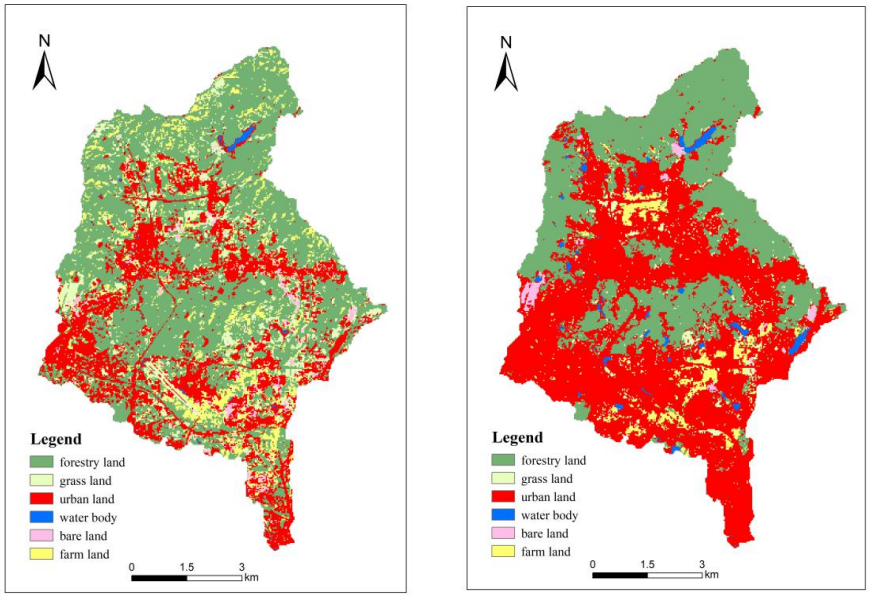

(**a**) (**b**)

Figure 4. LUC types of the Chebei Creek watershed. (**a**) 2015 automated LUC; (**b**) 2015 corrected LUC.

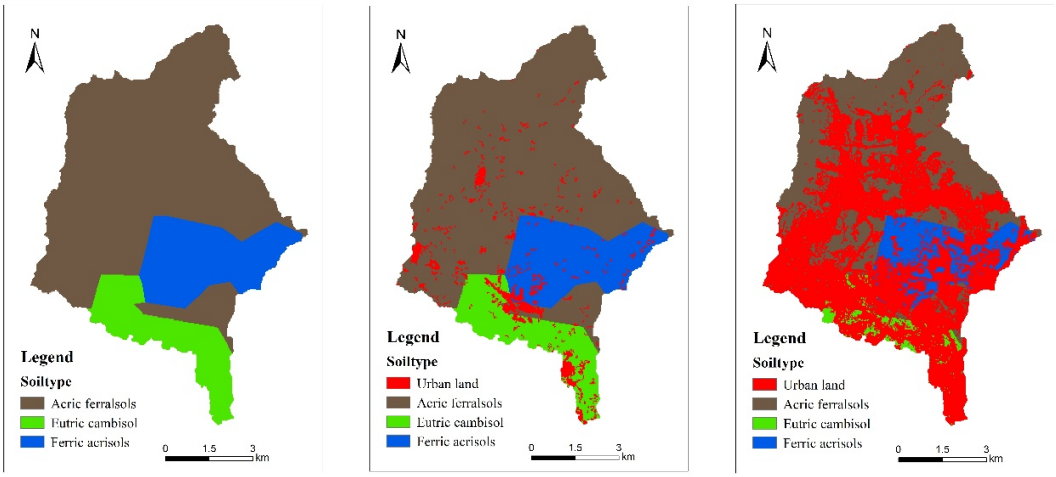

(**a**) (**b**) (**c**)

Figure 5. Soil map of the Chebei Creek watershed: (**a**) 1987 soil type map from the FAO dataset; (**b**) updated 1987 soil type map with estimated LUC; (**c**) 2015 soil type map with estimated LUC.

2.4. Hydrological Data

Four hydrological stations are located in the Chebei Creek watershed, namely, the South China Botanical Garden, Shaojiwo, Chebei Bridge, and Xibiankeng. Precipitation data from the rain gauges and discharge data from the Chebei Creek hydrological stations have been collected from March 2021 to the present. However, no rainfall data have been collected in Xibiankeng, and, thus, only hydrological data from the South China Botanical Garden, Shaojiwo, and Chebei Bridge sites were used to construct the Liuxihe model in the Chebei Creek watershed. After data screening and quality review, four observed flood events from 31 May 2021 to 23 June 2021 were identified and sorted, with an hourly temporal resolution. The Liuxihe model is a distributed hydrological model with physical significance, which derives model parameters physically from terrain characteristics. Therefore, only one flood event is needed for parameter optimization [53]. The flood designated as 2021060211 was selected for parameter optimization, and the

remaining three floods were used for model verification. Spatial interpolation of basin rainfall was conducted using the Thiessen polygon method, and grid-cell areal rainfall was generated according to the rainfall data obtained from rain gauges.

3. Model Implementation

3.1. Liuxihe Model Setup

The DEM produced in this study with a grid spatial resolution of 30 m was used to divide the study watershed into 72,175 grid cells, which were further divided into 758 river cells and 71,417 hill slope cells. No reservoir cells are present in the Chebei Creek watershed. The generation and confluence mechanisms of cells vary widely. If errors occur in the model structure, the simulation results will be distorted.

As the Chebei Bridge hydrological station is not located at the outlet point of the Chebei Creek watershed, flow data at the outlet point of the watershed cannot be verified by directly inputting the existing watershed area and hydrological station data into the Liuxihe model. Therefore, the watershed area must be adjusted. We used the Chebei Bridge hydrological station as the outlet point of the watershed to generate a new watershed area, designated as the Chebei Creek sub-watershed, as shown in Figure 6a. We clipped the DEM, land use, soil type, and other datasets to the sub-watershed scale and constructed a Liuxihe model for it.

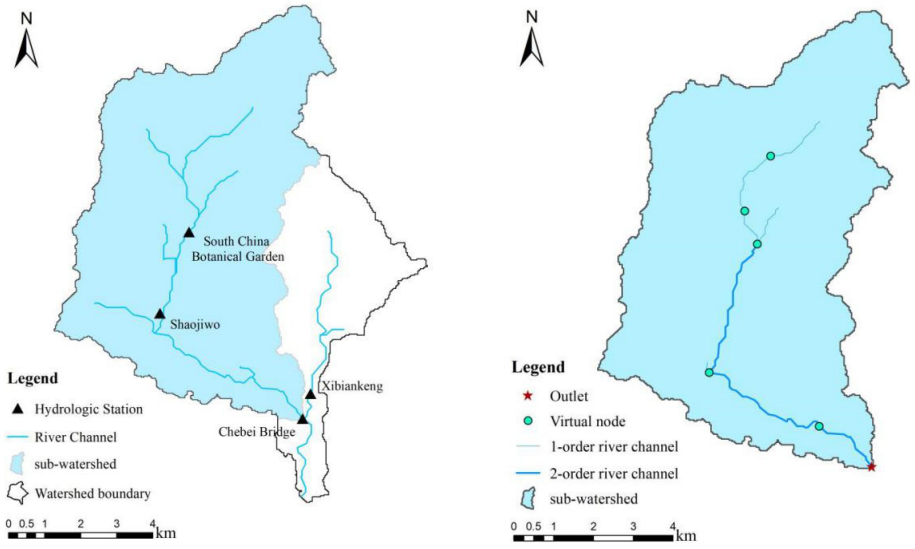

(**a**) (**b**)

Figure 6. Liuxihe model structures in the Chebei Creek watershed. (**a**) Spatial location of the Chebei Creek sub-watershed; (**b**) model structure based on the Chebei Creek sub-watershed.

A third-order river network was derived using the D8 method [75,76] and Strahler river ordering method [77] based on the DEM and then divided into seven virtual sections after setting five virtual nodes. In the Liuxihe model, the virtual river cross-section shape is assumed to be trapezoidal, with its size estimated from satellite remote sensing images. The results of unit classification, channel nodes, and virtual reaches are shown in Figure 6b.

3.2. Liuxihe Model Parameters

In the Liuxihe model, flow direction and slope are two topography-based model parameters and are derived using the D8 method [75,76] based on the DEM. The climate-based parameter of evaporation capacity was estimated to be 5 mm/day for all grid cells based on previous Liuxihe model applications in this region. Vegetation-based parameters include the evaporation coefficient and roughness [78]. According to previous Liuxihe

model parameterizations and references [79–83], a range of vegetation-based parameters was proposed, and their values are provided in Table 1.

Table 1. Vegetation-based parameter ranges and recommended values.

Vegetation Type	Range of Evaporation Coefficient (mm/d)	Recommended Evaporation Coefficient (mm/d)	Range of Roughness	Recommended Roughness
Forestry land	0.5–0.8	0.7	0.1–0.8	0.55
Grass land	0.5–0.7	0.6	0.01–0.4	0.18
Urban land	0.7–1.3	1.0	0.001–0.2	0.01
Bare land	0.2–0.6	0.4	0.005–0.3	0.12
Farm land	0.4–0.7	0.55	0.02–0.5	0.36

Six soil-based parameters were included: soil water content under saturated conditions, soil water content under field conditions, soil water content under wilting conditions, soil layer thickness, soil hydraulic conductivity at saturation, and soil characteristic coefficient. Based on previous reports [84–86], the soil water content at wilting is 30% of the soil water content under saturated conditions, the soil characteristic coefficient is 2.5, and the soil layer thickness estimates are listed in Table 2. The Soil Water Characteristics Hydraulic Properties Calculator proposed by Arya et al. [87] was employed to derive the soil water contents under saturated and field conditions as well as the hydraulic conductivity at saturation based on soil texture [88], organic matter, gravel content, salinity, and compaction; the estimated values are listed in Table 2.

Table 2. Soil-based parameters.

Soil Type	Soil Water Content under Saturated Conditions (%)	Soil Water Content under Field Conditions (%)	Soil Hydraulic Conductivity at Saturation (mm/h)	Soil Layer Thickness (mm)
Urban land	0.070	0.010	0.010	1
Acric Ferralsols	0.458	0.353	2.794	850
Eutric Cambisol	0.447	0.194	41.148	400
Ferric Acrisols	0.446	0.240	21.844	670

For grid cells containing urban land, the surface is impervious, and, thus, no infiltration occurs; all precipitation that reaches the ground is converted into surface runoff. To reflect this hydrological response of urban land, the soil-based parameters of urban land must be set to correspond to these characteristics. In this study, the soil water content at saturation was assigned a very small value, as listed in Table 2. A very small value for this parameter means that the soil can store very little water, and, therefore, most precipitation will not infiltrate the soil; it will instead become surface runoff.

3.3. Parameter Optimization of the Liuxihe Model

PSO [69] is a global search algorithm first proposed by American psychologist James Kennedy and electrical engineer Russell Eberhart in their studies of the social and intelligent behavior of bird flocks searching for food and good living conditions.

In this study, the PSO algorithm was used to optimize the model parameters. The population size (number of particles) of the particle swarm was 20, the number of evolutions was 50, and the total number of calculations was 1000. The value range of the inertia factor is [0.1, 0.9] and decreases linearly within this range for optimization; the value range of the learning acceleration factors C1 and C2 is [0.5, 2.5]. Optimization was performed dynamically and iteratively within the value range according to the arc cosine acceleration algorithm. Flood number 2021060211 was used to optimize the parameters of the Liuxihe model. Table 3 shows the parameter optimization results for the Liuxihe model, and Figure 7 shows the evolutionary results of the objective function value and parameter values obtained in the optimization process.

Table 3. Parameter optimization results for the Liuxihe model.

Parameters	**Soil Saturated Hydraulic Conductivity (Ks)**	**Slope Roughness (n)**	**Manning Coefficient (Mann)**	**Soil Layer Thickness (Zs)**	**Soil Characteristic Coefficient (b)**	**River Bottom Slope (Bs)**
	0.54	0.501	1.175	1.457	1.497	0.583
	River bottom width (Bw)	**Saturated water content (Csat)**	**Field capacity (Cfc)**	**Evaporation coefficient (v)**	**Wilting percentage (Cw)**	**Side slope grade (Ss)**
	1.393	1.492	0.505	1.327	1.378	1.46

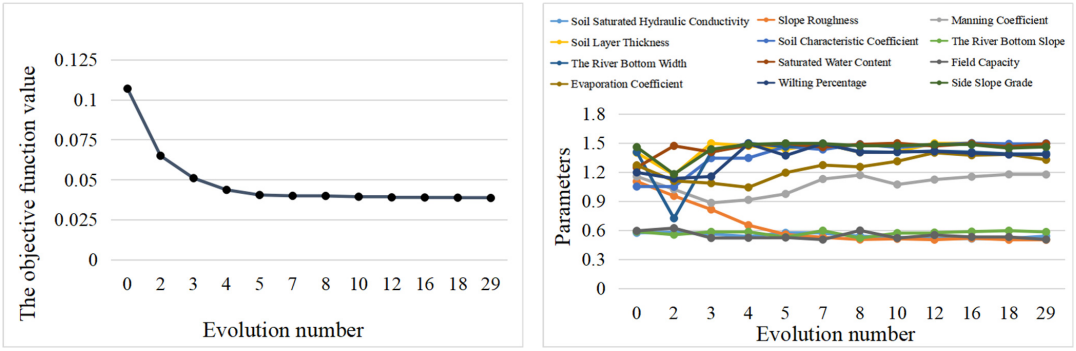

(**a**) (**b**)

Figure 7. Results of the parameter optimization of the Liuxihe model with the particle swarm optimization (PSO) algorithm. (**a**) Change curve of the objective function; (**b**) parameter evolution process.

After 29 evolutions of calculation, the value of the model objective function tended to be stable, and the model parameters generally converged to their optimal values. The parameter optimization effect obtained from the PSO algorithm was better than the initial parameter performance, indicating that the Liuxihe model parameter optimization improved the convergence speed.

3.4. Flood Simulation Results and Analysis

Chebei Creek is located in Tianhe District in eastern Guangzhou City. It is the largest river of seven rivers in Tianhe District. The basin has a relatively high degree of urbanization, and the prevention and control of urban waterlogging are difficult in this area. We conducted flood simulation experiments using four observed flood event datasets from 31 May 2021 to 23 June 2021, and general information about these floods is provided in Table 4. Flood number 2021060211 was selected for parameter optimization, and the remaining three floods were used for model verification.

Table 4. Information on the studied flood events.

Flood Event No.	Start Time (yyyymmddhh)	End Time (yyyymmddhh)	Duration (h)	Total Rainfall (mm)	Peak Flow (m^3/s)
2021053114	2021053114	2021060216	51	110.83	78.088
2021060211	2021060211	2021060323	37	36.77	61.206
2021061308	2021061308	2021061411	28	20.47	28.169
2021062203	2021062203	2021062305	27	31.90	52.207

The peak flow of flood No. 2021060211 was 61.206 m^3/s; after the optimization of the Liuxihe model parameters, it was 56.196 m^3/s, and the peak error was 8.2%. We also conducted a control experiment using the model without parameter optimization. The peak rate was 50.683 m^3/s, and the flood peak error was 17.2%, more than two times greater than the error with parameter optimization. Using the Liuxihe model parameters determined for the Chebei Creek flood simulation, the remaining three floods (Nos. 2021053114,

2021061308, and 2021062203) were simulated, and the hydrographs are shown in Figure 8. The simulated flood peak of No. 2021053114 was similar to the observed flood peak, and the simulated flood peak (the second peak) was predicted to occur 3 h earlier than the actual time. The peak error was 5.4%. The Nash–Sutcliffe coefficient is generally used to verify the quality of hydrological model simulation results. Values closer to 1 indicate the better quality and higher credibility of a model. The simulation results were generally consistent with the observed flood curve, with a Nash–Sutcliffe coefficient of 0.918, indicating that the simulation result of this flood is good. The simulated flood peak was smaller than the observed flood peak for No. 2021061308, but the temporal error was 0. The peak error was 24.6%. The simulated peak for No. 2021062203 was also lower than the observed peak flow. These results indicate that, in areas with high degrees of urbanization, the duration of the flood peak may be only 1 h, with the flood hydrograph showing a trend of a steep rise and fall. These characteristics impact flood modeling and forecasting in urbanized areas. The parameter statistics for each flood are listed in Table 5.

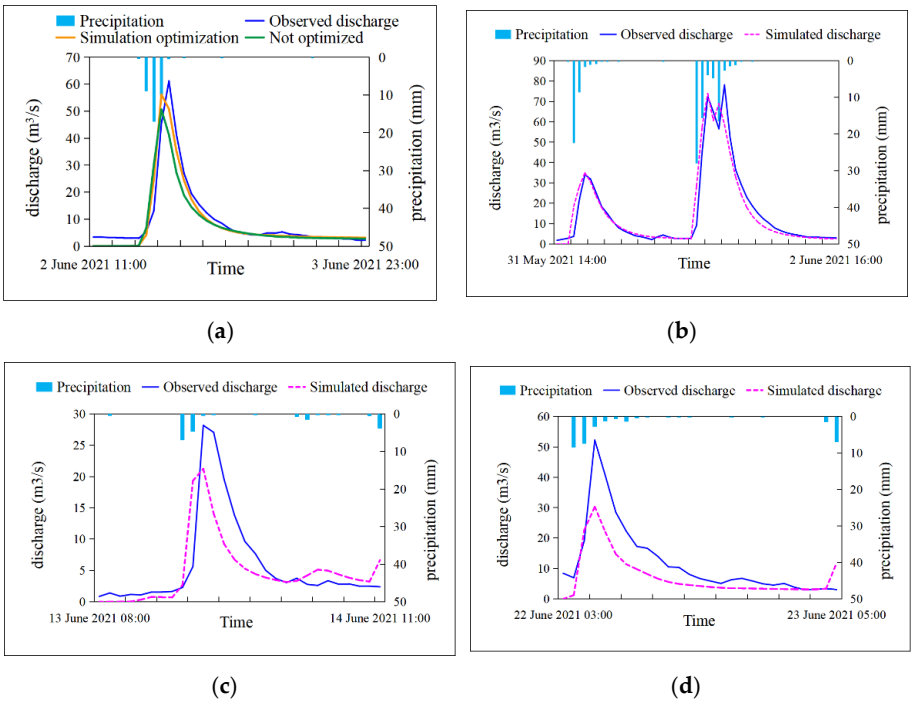

Figure 8. Parameter optimization and simulation processes for representative floods. (**a**) The parameter optimization flood (No. 2021060211); and the simulation floods: (**b**) No. 2021053114, (**c**) No. 2021061308, and (**d**) No. 2021062203.

Table 5. Statistical indicators of flood simulation results after the optimization of various Liuxihe model parameters.

Flood Event No.	Nash–Sutcliffe Coefficient	Water Balance Coefficient	Peak Flow Relative Error (%)	Peak Flow Duration Difference (h)
2021053114	0.918	0.987	5.4	−3.0
2021060211	0.920	0.909	8.2	−1.0
2021061308	0.576	0.838	24.6	0.0
2021062203	0.565	0.615	41.9	0.0

4. Results

4.1. Flood Forecasting in an Urbanized Watershed Using the Liuxihe Model

4.1.1. Forecast of the 15 June 2022 Flood

At 16:45 on 15 June 2022, the Sun Yat-sen University Smart Flood Disaster Prevention and Control Technology Team observed that the river water level rose and the river flow

increased in the urban rainstorm and flood monitoring system installed in the Chebei Creek watershed. Heavy rain was expected over the next few hours. The team immediately decided to begin flood forecasting for the watershed using the Liuxihe model, monitored rainfall and flood flows in the watershed in real time, and began flood forecasting when the forecast start conditions were met.

At 17:30 on 15 June 2022, the flow at Chebei Bridge Station reached 32.075 m^3/s, and the water began to rise. After downloading the data from the monitoring system, the team analyzed the data rapidly and input the sorted flood forecast data files to the Liuxihe model Cloud Computing and Service Platform to forecast flooding in the watershed. The first round of forecasting results was released at 18:38. The forecast was based on rainfall as of 18:00. The forecasted and observed flows are shown in Figure 9a. The forecast period for this forecast was 5 h. At 20:28, the team downloaded the latest flood data, including the rainfall and flow data from three rainfall stations at 19:00 and 20:00. The team conducted and released the second round of rolling forecast results at 20:34. The forecast results were based on rainfall as of 20:00. The predicted and observed flows are shown in Figure 9b. At 21:42, the team downloaded the latest flood data and conducted the third round of rolling forecasting. The results were released at 21:49. The predicted and observed flows at that time are shown in Figure 9c.

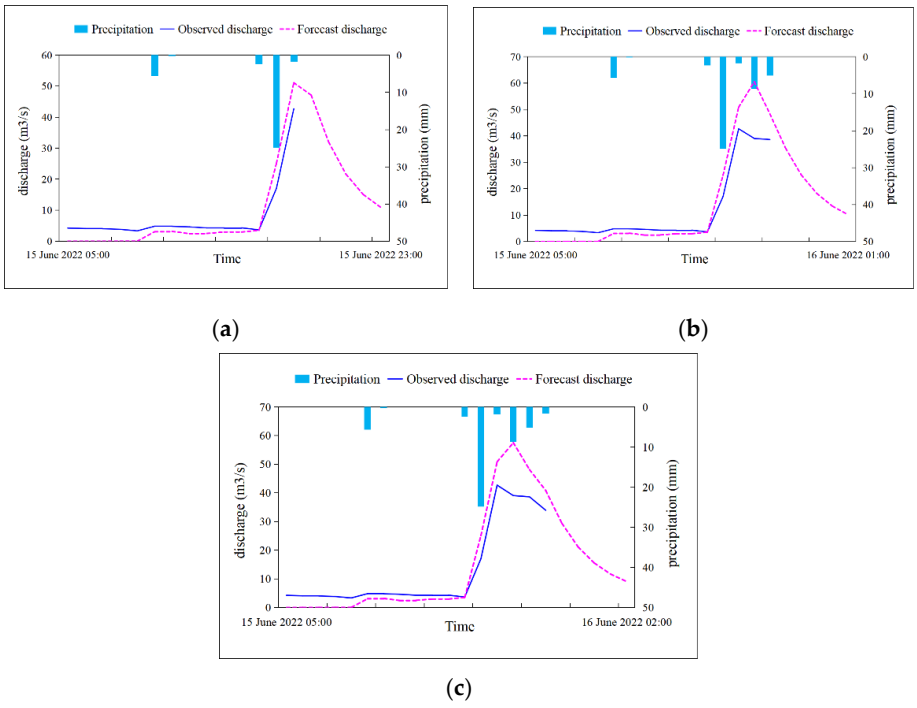

Figure 9. Three rounds of forecasts for the flood 15 June 2022. (**a**) First-round forecast results; (**b**) second-round rolling forecast results; and (**c**) third-round rolling forecast results.

The observed peak flow of this flood was 42.713 m^3/s, the predicted peak flow was 50.878 m^3/s, and the forecast accuracy of the peak flow was 83.95%. The observed flood peak occurred at 18:00 on 15 June 2022, the predicted flood peak was at 19:00 on 15 June 2022, and, thus, the predicted peak was delayed by 1 h. The forecast period for the flood peak is 5 h. According to the specifications set for hydrological information forecasting, this flood forecast is sufficiently accurate.

4.1.2. Forecast of the 2 July 2022 Flood

At 14:15 on 2 July 2022, the same team mentioned above observed a rise in the river water level and an increase in the river flow at the urban rainstorm and flood monitoring system in the Chebei Creek watershed. However, monitoring continued until 12:20 on

3 July, when the flow rate at Chebei Bridge Station had not exceeded 30 m^3/s and thus did not meet the forecast start conditions. At 12:25, the flow rate at the station exceeded 30 m^3/s. The team immediately began monitoring rainfall and flood flows in the watershed in real time and began flood forecasting when the forecast start conditions were met.

At 14:00, the flow at the station reached 119.766 m^3/s, and the water level was rising rapidly. After downloading the data from the system, the team analyzed the data in real time and began forecasting. The first round of forecast results was released at 14:36 on 3 July 2022. That forecast was based on rainfall at the rainfall station and flow at Chebei Bridge Station as of 14:00 on 3 July 2022. The forecast and observed flows are shown in Figure 10a. The forecast period for this forecast was 5 h. At 16:08 on 3 July 2022, the Sun Yat-Sen University research team downloaded the latest flood data, including rainfall and flow data for three rainfall stations at 15:00 and 16:00 on July 3. The team conducted the second round of rolling forecasting for the Chebei Creek watershed using the Liuxihe model Cloud Computing and Service Platform and released the second round of rolling forecast results at 16:16 on 3 July 2022. These forecast results were based on rainfall at the rainfall station and flow at Chebei Bridge Station as of 16:00 on 3 July 2022. The predicted and observed flows are shown in Figure 10b. The second round of rolling forecast results showed that the flood flow decreased after 16:00 on 3 July 2022, and, therefore, we decided to end the flood forecast for this event. However, at 20:00 on 3 July, flooding resumed, and a small flood peak occurred. We then decided to continue flood forecasting for the second flood peak. The team downloaded the latest flood data and conducted the third round of rolling forecasting for the Chebei Creek watershed. The third-round forecast results were released at 22:47 on 3 July 2022. The forecast and observed flows are shown in Figure 10c.

The observed peak flow of this flood was 119.766 m^3/s, the predicted flood peak flow was 116.245 m^3/s, and, thus, the forecast accuracy of the peak flow is 97.06%. The observed flood peak occurred at 14:00 on 3 July 2022, and the predicted flood peak occurred on 3 July 2022, at 13:00 on Sunday, and, thus, the forecast peak time is 1 h ahead; the flood peak forecast period was 5 h. According to the specifications set for hydrological information forecasting, this flood forecast was sufficiently accurate.

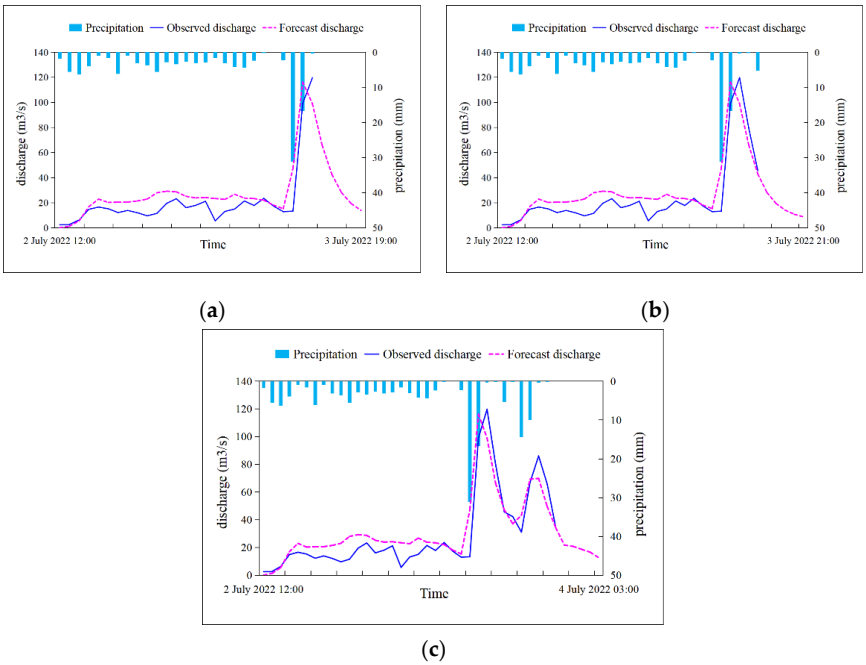

Figure 10. Three rounds of forecasts for the flood 2 July 2022. (**a**) First-round forecast results; (**b**) second-round rolling forecast results; and (**c**) third-round rolling forecast results.

5. Discussion

In 2022, the Liuxihe model was used twice for flood forecasting in the urbanized watershed of Chebei Creek, and both forecasts achieved good results. Line graphs of the progression of each flood showed steep rises and falls, and the second flood had two flood peaks, complicating forecasting. Flood No. 20220615 had rainfall in the basin that continued after the observed flood peak, when the observed flow had begun to decrease. The predicted pattern of the flow and flood process was more reasonable for this flood, which may be related to the uneven spatial distribution of rainfall. In this forecast, due to the failure of Shaojiwo station, one of the three rainfall stations in the Chebei Creek watershed, fewer data were available, which undoubtedly affected the forecast accuracy for this flood. Less than an hour was needed for the observed flow of flood No. 20220702 to increase from less than 20 m^3/s to nearly 100 m^3/s. After reaching the flood peak, the flow fell rapidly, and a second flood peak occurred, which increased the difficulty of forecasting.

Most previous research using the Liuxihe model has addressed flood simulation in natural basins. The application of the Liuxihe model in areas affected by impacts of snow cover [89,90] and snowline elevation [91] on the hydrological process and climate, as well as semi-arid areas [92,93] and arid areas [94–96], has been scarce. Wang [55] applied the Liuxihe model to an urbanized watershed but remained in the stage of flood simulation. This study was the first to apply the Liuxihe model to real-time flood forecasting in an urbanized watershed. The forecast accuracies were 83.95% and 97.06% for floods No. 20220615 and No. 20220702, respectively, and the temporal difference between the forecast and observed peaks was 1 h (delayed or advanced), demonstrating excellent performance. The following issues require further improvement:

(i) As noted above, real-time flood forecasting in an urbanized watershed requires timely and stable rainfall station data. A problem with the station data will greatly reduce the accuracy of forecasts.
(ii) Although the PBDHM and refined underlying surface data of the watershed were prepared, real-time flood forecasting still relied on a cloud computing platform with a powerful calculation ability. In addition, the timely mobilization and deployment of operators is key to real-time flood forecasting.
(iii) Real-time flood forecasting requires the consistent maintenance of rainfall station equipment. Rainfall stations in urbanized watersheds are generally powered by solar energy to maintain equipment operation. However, a heavy rainstorm in an urbanized watershed, particularly one in which rainfall continues for a long time, may affect the normal operation of the equipment and the stability of the data transmission signal.

6. Conclusions

A typical watershed in Guangzhou, the Chebei Creek watershed, was used as a study area for the simulation of the flood process in an urbanized area with a distributed hydrological model, the Liuxihe model. At the same time, using remote sensing images obtained by the Landsat satellite in 2015, we used the DT C4.5 automatic classification method to quantitatively estimate the LUC changes in the watershed, along with a visual interpretation method to correct the estimation results. The results with and without Liuxihe model parameter optimization were analyzed and compared. Finally, using the optimized model parameters, two floods in the Chebei Creek watershed in 2022 were forecasted in real time, and satisfactory results were obtained.

1. The flood process in the watershed at different rainfall intensities was simulated. Using the optimized parameters, three floods (large, medium, and small) were simulated. From the simulation results, areas with a high degree of urbanization had a flood peak duration of only 1 h, and the flood water level line showed a sharp rising and falling pattern. These findings will improve flood modeling and forecasting in urbanized areas.
2. The 15 June 2022 flood was the first flood in the Chebei Creek River Basin in 2022. The flood rose and fell sharply, complicating forecasting. Rain continued after the observed

flood peak of this flood, when the observed flow had begun to fall. In addition, during this forecast, Shaojiwo station, one of three rainfall stations in the Chebei Creek watershed, experienced a failure and produced no data, which undoubtedly affected the forecast accuracy. The Liuxihe model had a forecast accuracy of 83.95% for the peak flow of this flood.

3. The 2 July 2022 flood was the second one. It also rose and fell sharply and showed two peaks, further hampering forecasting efforts. The observed flow of the flood rose from less than 20 m^3/s to nearly 100 m^3/s in less than an hour. After reaching the flood peak, it quickly fell, and a second flood peak appeared, which increased the difficulty of forecasting. The model had a forecast accuracy of 97.06%, and the peak was 1 h ahead of the observed peak.
4. The Liuxihe model is a PBDHM that can meet the accuracy requirements for flood flow forecasting to support reservoir flood control operations. It requires the optimization of its parameters. Model parameters derived from physical data have uncertainty, and the performance of the model can be significantly improved through optimization. The two flood forecasting results presented in this study achieved a high accuracy, demonstrating the excellent performance of the Liuxihe model for real-time flood forecasting in urbanized watersheds such as Chebei Creek.

Author Contributions: Y.C. was responsible for proposing the original idea and providing technical guidance; Y.G. was responsible for the data compilation, processing, computation, and writing; H.S. and J.L. were responsible for the data sorting; H.S. and J.L. were responsible for the data curation; Y.G. was responsible for writing the original draft; Y.C. was responsible for reviewing and editing. All authors have read and agreed to the published version of the manuscript.

Funding: This study was supported by the National Natural Science Foundation of China (NSFC) (no. 51961125206) and the Science and Technology Program of Guangdong Province (no. 2020B1515120079).

Data Availability Statement: Data sharing is not applicable.

Conflicts of Interest: The authors declare no conflict of interest regarding the publication of this paper.

References

1. United Nations Population Division (UNPD). World Population Prospects, the 2010 Revision. New York: United Nations. Available online: http://esa.un.org/wpp (accessed on 25 November 2022).
2. Rounsevell, M.; Reginster, I.; Araújo, M.; Carter, T.; Dendoncker, N.; Ewert, F.; House, J.; Kankaanpää, S.; Leemans, R.; Metzger, M.; et al. A coherent set of future land use change scenarios for Europe. *Agric. Ecosyst. Environ.* **2006**, *114*, 57–68. [CrossRef]
3. Jedwab, R.; Christiaensen, L.; Gindelsky, M. Demography, urbanization and development: Rural push, urban pull and urban push? *J. Urban Econ.* **2017**, *98*, 6–16. [CrossRef]
4. Hollis, G.E. The effect of urbanization on floods of different recurrence interval. *Water Resour. Res.* **1975**, *11*, 431–435. [CrossRef]
5. Poff, N.L.; Bledsoe, B.P.; Cuhaciyan, C.O. Hydrologic variation with land use across the contiguous United States: Geomorphic and ecological consequences for stream ecosystems. *Geomorphology* **2006**, *79*, 264–285. [CrossRef]
6. Yira, Y.; Diekkrüger, B.; Steup, G.; Bossa, A. Modeling land use change impacts on water resources in a tropical West African catchment (Dano, Burkina Faso). *J. Hydrol.* **2016**, *537*, 187–199. [CrossRef]
7. Luo, P.; Zheng, Y.; Wang, Y.; Zhang, S.; Yu, W.; Zhu, X.; Huo, A.; Wang, Z.; He, B.; Nover, D. Comparative Assessment of Sponge City Constructing in Public Awareness, Xi'an, China. *Sustainability* **2022**, *14*, 11653. [CrossRef]
8. Shen, L.; Kyllo, J.M.; Guo, X. An Integrated Model Based on a Hierarchical Indices System for Monitoring and Evaluating Urban Sustainability. *Sustainability* **2013**, *5*, 524–559. [CrossRef]
9. Luo, P.; Liu, L.; Wang, S.; Ren, B.; He, B.; Nover, D. Influence assessment of new Inner Tube Porous Brick with absorbent concrete on urban floods control. *Case Stud. Constr. Mater.* **2022**, *17*, e01236. [CrossRef]
10. Zha, X.; Luo, P.; Zhu, W.; Wang, S.; Lyu, J.; Zhou, M.; Huo, A.; Wang, Z. A bibliometric analysis of the research on Sponge City: Current situation and future development direction. *Ecohydrology* **2021**, *14*, e2328. [CrossRef]
11. Shaw, S.B.; Marrs, J.; Bhattarai, N.; Quackenbush, L. Longitudinal study of the impacts of land cover change on hydrologic response in four mesoscale watersheds in New York State, USA. *J. Hydrol.* **2014**, *519*, 12–22. [CrossRef]
12. Zhu, W.; Zha, X.; Luo, P.; Wang, S.; Cao, Z.; Lyu, J.; Zhou, M.; He, B.; Nover, D. A quantitative analysis of research trends in flood hazard assessment. *Stoch. Environ. Res. Risk Assess.* **2022**. [CrossRef]

13. Hu, Y.; Duan, W.; Chen, Y.; Zou, S.; Kayumba, P.M.; Qin, J. Exploring the changes and driving forces of water footprint in Central Asia: A global trade assessment. *J. Clean. Prod.* **2022**, *375*, 134062. [CrossRef]
14. Karlsson, I.B.; Sonnenborg, T.O.; Refsgaard, J.C.; Trolle, D.; Børgesen, C.D.; Olesen, J.E.; Jeppesen, E.; Jensen, K.H. Combined effects of climate models, hydrological model structures and land use scenarios on hydrological impacts of climate change. *J. Hydrol.* **2016**, *535*, 301–317. [CrossRef]
15. Hurkmans, R.T.W.L.; Terink, W.; Uijlenhoet, R.; Moors, E.J.; Troch, P.A.; Verburg, P.H. Effects of land use changes on streamflow generation in the Rhine basin. *Water Resour. Res.* **2009**, *45*, W06405. [CrossRef]
16. Crawford, N.H.; Linsley, R.K. *Digital Simulation in Hydrology'Stanford Watershed Model 4*; Technical Report No. 39; Department of Civil Engineering, Stanford University: Stanford, CA, USA, 1966.
17. Zhao, R.-J. *Watershed Hydrological Simulation—Xinanjiang Model and Northern Shaanxi Model*; Electric Power Press: Beijing, China, 1983.
18. Lørup, J.K.; Refsgaard, J.C.; Mazvimavi, D. Assessing the effect of land use change on catchment runoff by combined use of statistical tests and hydrological modelling: Case studies from Zimbabwe. *J. Hydrol.* **1998**, *205*, 147–163. [CrossRef]
19. Hundecha, Y.; Bárdossy, A. Modeling of the effect of land use changes on the runoff generation of a river basin through parameter regionalization of a watershed model. *J. Hydrol.* **2004**, *292*, 281–295. [CrossRef]
20. Shi, P.-J.; Yuan, Y.; Zheng, J.; Wang, J.-A.; Ge, Y.; Qiu, G.-Y. The effect of land use/cover change on surface runoff in Shenzhen region, China. *Catena* **2007**, *69*, 31–35. [CrossRef]
21. Ashagrie, A.G.; de laat, P.J.M.; de Wit, M.J.M.; Tu, M.; Uhlenbrook, S. Detecting the influence of land use changes on discharges and floods in the Meuse River Basin—The predictive power of a ninety-year rainfall-runoff relation? *Hydrol. Earth Syst. Sci.* **2006**, *10*, 691–701. [CrossRef]
22. Saghafian, B.; Farazjoo, H.; Bozorgy, B.; Yazdandoost, F. Flood Intensification due to Changes in Land Use. *Water Resour. Manag.* **2007**, *22*, 1051–1067. [CrossRef]
23. Suriya, S.; Mudgal, B. Impact of urbanization on flooding: The Thirusoolam sub watershed—A case study. *J. Hydrol.* **2012**, *412–413*, 210–219. [CrossRef]
24. Zhou, F.; Xu, Y.; Chen, Y.; Xu, C.-Y.; Gao, Y.; Du, J. Hydrological response to urbanization at different spatio-temporal scales simulated by coupling of CLUE-S and the SWAT model in the Yangtze River Delta region. *J. Hydrol.* **2013**, *485*, 113–125. [CrossRef]
25. Miller, J.D.; Kim, H.; Kjeldsen, T.R.; Packman, J.; Grebby, S.; Dearden, R. Assessing the impact of urbanization on storm runoff in a pen-urban catchment using historical change in impervious cover. *J. Hydrol.* **2014**, *515*, 59–70. [CrossRef]
26. Baker, T.J.; Miller, S.N. Using the Soil and Water Assessment Tool (SWAT) to assess land use impact on water resources in an East African watershed. *J. Hydrol.* **2013**, *486*, 100–111. [CrossRef]
27. Huang, H.; Cheng, S.; Wen, J.; Lee, J. Effect of growing watershed imperviousness on hydrograph parameters and peak discharge. *Hydrol. Process.* **2008**, *22*, 2075–2085. [CrossRef]
28. Du, J.; Qian, L.; Rui, H.; Zuo, T.; Zheng, D.; Xu, Y.; Xu, C.-Y. Assessing the effects of urbanization on annual runoff and flood events using an integrated hydrological modeling system for Qinhuai River basin, China. *J. Hydrol.* **2012**, *464*, 127–139. [CrossRef]
29. Duan, W.; Maskey, S.; Chaffe, P.L.; Luo, P.; He, B.; Wu, Y.; Hou, J. Recent Advancement in Remote Sensing Technology for Hydrology Analysis and Water Resources Management. *Remote. Sens.* **2021**, *13*, 1097. [CrossRef]
30. Bai, H.; Li, Z.; Guo, H.; Chen, H.; Luo, P. Urban Green Space Planning Based on Remote Sensing and Geographic Information Systems. *Remote Sens.* **2022**, *14*, 4213. [CrossRef]
31. Chen, K.-S. *Principles of Synthetic Aperture Radar Imaging: A System Simulation Approach*; CRC Press: Boca Raton, FL, USA, 2016; Volume 2.
32. Jackson, C.R.; Apel, J.R. *Synthetic Aperture Radar: Marine User's Manual*; NOAA: Washington, DC, USA, 2004.
33. Treitz, P.M.; Howarth, P.J.; Gong, P. Application of satellite and GIS technologies for land-cover and land-use mapping at the rural-urban fringe: A case study. *Photogramm. Eng. Remote Sens.* **1992**, *58*, 439–448.
34. Irons, J.R.; Dwyer, J.L.; Barsi, J.A. The next Landsat satellite: The Landsat Data Continuity Mission. *Remote. Sens. Environ.* **2012**, *122*, 11–21. [CrossRef]
35. Cao, Z.; Zhu, W.; Luo, P.; Wang, S.; Tang, Z.; Zhang, Y.; Guo, B. Spatially Non-Stationary Relationships between Changing Environment and Water Yield Services in Watersheds of China's Climate Transition Zones. *Remote. Sens.* **2022**, *14*, 5078. [CrossRef]
36. Pal, M.; Mather, P.M. An assessment of the effectiveness of decision tree methods for land cover classification. *Remote. Sens. Environ.* **2003**, *86*, 554–565. [CrossRef]
37. Kavzoglu, T.; Mather, P.M. The use of backpropagating artificial neural networks in land cover classification. *Int. J. Remote. Sens.* **2003**, *24*, 4907–4938. [CrossRef]
38. Mazzoni, D.; Garay, M.J.; Davies, R.; Nelson, D. An operational MISR pixel classifier using support vector machines. *Remote Sens. Environ.* **2007**, *107*, 149–158. [CrossRef]
39. Nigam, K.; McCallum, A.K.; Thrun, S.; Mitchell, T. Text Classification from Labeled and Unlabeled Documents using EM. *Mach. Learn.* **2000**, *39*, 103–134. [CrossRef]
40. Yang, C.; Bruzzone, L.; Sun, F.; Lu, L.; Guan, R.; Liang, Y. A Fuzzy-Statistics-Based Affinity Propagation Technique for Clustering in Multispectral Images. *IEEE Trans. Geosci. Remote Sens.* **2010**, *48*, 2647–2659. [CrossRef]
41. Biggio, B.; Fumera, G.; Roli, F. Multiple classifier systems for robust classifier design in adversarial environments. *Int. J. Mach. Learn. Cybern.* **2010**, *1*, 27–41. [CrossRef]

42. Chen, Y.; Dou, P.; Yang, X. Improving Land Use/Cover Classification with a Multiple Classifier System Using AdaBoost Integration Technique. *Remote Sens.* **2017**, *9*, 1055. [CrossRef]
43. Freeze, R.; Harlan, R. Blueprint for a physically-based, digitally-simulated hydrologic response model. *J. Hydrol.* **1969**, *9*, 237–258. [CrossRef]
44. Im, S.; Kim, H.; Kim, C.; Jang, C. Assessing the impacts of land use changes on watershed hydrology using MIKE SHE. *Environ. Earth Sci.* **2008**, *57*, 231–239. [CrossRef]
45. Abbott, M.; Bathurst, J.; Cunge, J.; O'connell, P.; Rasmussen, J. An introduction to the European Hydrological System—Systeme Hydrologique Europeen,"SHE", 2: Structure of a physically-based, distributed modelling system. *J. Hydrol.* **1986**, *87*, 61–77. [CrossRef]
46. Liang, X.; Lettenmaier, D.P.; Wood, E.F.; Burges, S.J. A simple hydrologically based model of land surface water and energy fluxes for general circulation models. *J. Geophys. Res. Atmos.* **1994**, *99*, 14415–14428. [CrossRef]
47. Wigmosta, M.S.; Vail, L.W.; Lettenmaier, D.P. A distributed hydrology-vegetation model for complex terrain. *Water Resour. Res.* **1994**, *30*, 1665–1679. [CrossRef]
48. Wang, Z.-M.; Batelaan, O.; De Smedt, F. A distributed model for water and energy transfer between soil, plants and atmosphere (WetSpa). *Phys. Chem. Earth* **1996**, *21*, 189–193. [CrossRef]
49. Chormanski, J.; Van de Voorde, T.; De Roeck, T.; Batelaan, O.; Canters, F. Improving Distributed Runoff Prediction in Urbanized Catchments with Remote Sensing based Estimates of Impervious Surface Cover. *Sensors* **2008**, *8*, 910–932. [CrossRef] [PubMed]
50. Yang, D.; Herath, S.; Musiake, K. Development of a geomorphologic properties extracted from DEMs for hydrologic modeling. *Annu. J. Hydraul. Eng. JSCE* **1997**, *47*, 49–65.
51. Jia, Y.; Ni, G.; Kawahara, Y.; Suetsugi, T. Development of WEP model and its application to an urban watershed. *Hydrol. Process.* **2001**, *15*, 2175–2194. [CrossRef]
52. Kavvas, M.L.; Chen, Z.Q.; Dogrul, C.; Yoon, J.Y.; Ohara, N.; Liang, L.; Aksoy, H.; Anderson, M.L.; Yoshitani, J.; Fukami, K.; et al. Watershed Environmental Hydrology (WEHY) Model Based on Upscaled Conservation Equations: Hydrologic Module. *J. Hydrol. Eng.* **2004**, *9*, 450–464. [CrossRef]
53. Chen, Y.; Ren, Q.; Huang, F.; Xu, H.; Cluckie, I. Liuxihe Model and Its Modeling to River Basin Flood. *J. Hydrol. Eng.* **2011**, *16*, 33–50. [CrossRef]
54. Beven, K. 12 Equifinality and uncertainty in geomorphological modelling. In *The Scientific Nature of Geomorphology: Proceedings of the 27th Binghamton Symposium in Geomorphology, Held 27–29 September 1996*; John Wiley & Sons: Hoboken, NJ, USA, 1996.
55. Wang, H.; Chen, Y. Identifying Key Hydrological Processes in Highly Urbanized Watersheds for Flood Forecasting with a Distributed Hydrological Model. *Water* **2019**, *11*, 1641. [CrossRef]
56. Siriwardena, L.; Finlayson, B.; McMahon, T. The impact of land use change on catchment hydrology in large catchments: The Comet River, Central Queensland, Australia. *J. Hydrol.* **2006**, *326*, 199–214. [CrossRef]
57. Zheng, J.; Fang, W.; Shi, P.; Zhuo, L. Modeling the impacts of land use change on hydrological processes in fast urbanizing region—A case study of the Buji watershed in Shenzhen city. *J. Nat. Resour.* **2009**, *24*, 1560–1572.
58. Hejazi, M.I.; Markus, M. Impacts of Urbanization and Climate Variability on Floods in Northeastern Illinois. *J. Hydrol. Eng.* **2009**, *14*, 606–616. [CrossRef]
59. Olivera, F.; DeFee, B.B. Urbanization and Its Effect On Runoff in the Whiteoak Bayou Watershed, Texas1. *JAWRA J. Am. Water Resour. Assoc.* **2007**, *43*, 170–182. [CrossRef]
60. Li, Y.; Wang, C. Impacts of Urbanization on Surface Runoff of the Dardenne Creek Watershed, St. Charles County, Missouri. *Phys. Geogr.* **2009**, *30*, 556–573. [CrossRef]
61. Grove, M.; Harbor, J.; Engel, B.; Muthukrishnan, S. Impacts of urbanization on surface hydrology, Little Eagle Creek, Indiana, and analysis of LTHIA model sensitivity to data resolution. *Phys. Geogr.* **2001**, *22*, 135–153. [CrossRef]
62. Getachew, H.E.; Melesse, A.M. The impact of land use change on the hydrology of the Angereb Watershed, Ethiopia. *Int. J. Water Sci.* **2012**, *1*, 4.
63. Luo, P.; Xu, C.; Kang, S.; Huo, A.; Lyu, J.; Zhou, M.; Nover, D. Heavy metals in water and surface sediments of the Fenghe River Basin, China: Assessment and source analysis. *Water Sci. Technol.* **2021**, *84*, 3072–3090. [CrossRef]
64. Cao, Z.; Wang, S.; Luo, P.; Xie, D.; Zhu, W. Watershed Ecohydrological Processes in a Changing Environment: Opportunities and Challenges. *Water* **2022**, *14*, 1502. [CrossRef]
65. Luo, P.; Mu, Y.; Wang, S.; Zhu, W.; Mishra, B.K.; Huo, A.; Zhou, M.; Lyu, J.; Hu, M.; Duan, W.; et al. Exploring sustainable solutions for the water environment in Chinese and Southeast Asian cities. *Ambio* **2021**, *51*, 1199–1218. [CrossRef]
66. Duan, W.; Zou, S.; Chen, Y.; Nover, D.; Fang, G.; Wang, Y. Sustainable water management for cross-border resources: The Balkhash Lake Basin of Central Asia, 1931–2015. *J. Clean. Prod.* **2020**, *263*, 121614. [CrossRef]
67. Chen, Y. *Liuxihe Model*; Science Press: Beijing, China, 2009; p. 198.
68. Chen, Y.; Dong, Y.; Zhang, P. Study on the method of flood forecasting of small and medium sized catchment. In Proceedings of the 2013 Meeting of the Chinese Society of Hydraulic Engineering, Guangzhou, China, 26–28 November 2013; pp. 26–28.
69. Chen, Y.; Li, J.; Xu, H. Improving flood forecasting capability of physically based distributed hydrological models by parameter optimization. *Hydrol. Earth Syst. Sci.* **2016**, *20*, 375–392. [CrossRef]
70. Deng, H.; Pepin, N.C.; Chen, Y.; Guo, B.; Zhang, S.; Zhang, Y.; Chen, X.; Gao, L.; Meibing, L.; Ying, C. Dynamics of Diurnal Precipitation Differences and Their Spatial Variations in China. *J. Appl. Meteorol. Clim.* **2022**, *61*, 1015–1027. [CrossRef]

71. Yi-yang, X.I.E.; Da-ming, L.I.; Pei-yan, L.I.; Shu-qin, S.H.E.N.; Jian-min, Y.I.N.; Su-qin, H.A.N.; Ming-jian, Z.E.N.G.; Xiao-qing, G.U. Research and application of numerical model for urban storm urban flooding. *Adv. Water Sci.* **2005**, *16*, 384–390.
72. Zhou, H.; Wang, C. Guangdong Dongguan city urban flooding causes analysis and prevention measures. *China Flood Drought Manag.* **2013**, *23*, 70–71.
73. Luo, P.; Luo, M.; Li, F.; Qi, X.; Huo, A.; Wang, Z.; He, B.; Takara, K.; Nover, D.; Wang, Y. Urban flood numerical simulation: Research, methods and future perspectives. *Environ. Model. Softw.* **2022**, *156*, 105478. [CrossRef]
74. Duan, W.; Zou, S.; Christidis, N.; Schaller, N.; Chen, Y.; Sahu, N.; Li, Z.; Fang, G.; Zhou, B. Changes in temporal inequality of precipitation extremes over China due to anthropogenic forcings. *npj Clim. Atmos. Sci.* **2022**, *5*, 33. [CrossRef]
75. O'Callaghan, J.F.; Mark, D.M. The extraction of drainage networks from digital elevation data. *Comput. Vis. Graph. Image Process.* **1984**, *28*, 323–344. [CrossRef]
76. Jenson, S.K.; Domingue, J.O. Extracting topographic structure from digital elevation data for geographic information system analysis. *Photogramm. Eng. Remote Sens.* **1988**, *54*, 1593–1600.
77. Strahler, A.N. Quantitative analysis of watershed geomorphology. *Eos Trans. Am. Geophys. Union* **1957**, *38*, 913–920. [CrossRef]
78. Wei, X.; Yang, J.; Luo, P.; Lin, L.; Lin, K.; Guan, J. Assessment of the variation and influencing factors of vegetation NPP and carbon sink capacity under different natural conditions. *Ecol. Indic.* **2022**, *138*, 108834. [CrossRef]
79. Huiquan, C.; Shimin, M. Calculation and verification of an universal water surface evaporation coefficient formula. *Adv. Water Sci.* **1995**, *6*, 116–120.
80. Zhang, S.; Xu, D.; Li, Y.; Cai, L. An optimized inverse model used to estimate Kostiakov infiltration parameters and Manning's roughness coefficient based on SGA and SRFR model:(I) establishment. *J. Hydraul. Eng.* **2006**, *37*, 1297–1302.
81. Shaohui, Z.; Di, X.U.; Yinong, L.I.; Lingen, C.A.I. Optimized inverse model used to estimate Kostiakov infiltration parameters and Manning's roughness coefficient based on SGA and SRFR model: II Application. *J. Hydraul. Eng.* **2007**, *38*, 402–408.
82. Guo, H.; Han, Y.; Bai, X. Hydrological Effects of Littet on Different Forest Stands and Study about Surface Roughness Coefficient. *J. Soil Water Conserv.* **2010**, *24*, 179–183.
83. Li, Y.; Zhang, J.; Ru, H.; Li, M.; Wang, D.; Ding, Y. Effect of Different Land Use Types on Soil Anti-scourability and Roughness in Loess Area of Western Shanxi Province. *J. Soil Water Conserv.* **2013**, *27*, 1–6, 28.
84. Anderson, A.N.; McBratney, A.B.; FitzPatrick, E.A. Soil Mass, Surface, and Spectral Fractal Dimensions Estimated from Thin Section Photographs. *Soil Sci. Soc. Am. J.* **1996**, *60*, 962–969. [CrossRef]
85. Qiong, S.; Shuanghe, S.; Ze, G.U. Conversion Coefficient between Small Evaporation Pan and Theoretically Calculated Water Surface Evaporation in China. *J. Nanjing Inst. Meteorol.* **2007**, *30*, 561–565.
86. Zhang, H.; Chen, Y.; Zhou, J. Assessing the long-term impact of urbanization on run-off using a remote-sensing-supported hydrological model. *Int. J. Remote Sens.* **2015**, *36*, 5336–5352. [CrossRef]
87. Arya, L.M.; Paris, J.F. A Physicoempirical Model to Predict the Soil Moisture Characteristic from Particle-Size Distribution and Bulk Density Data. *Soil Sci. Soc. Am. J.* **1981**, *45*, 1023–1030. [CrossRef]
88. Wang, Z.; Luo, P.; Zha, X.; Xu, C.; Kang, S.; Zhou, M.; Nover, D.; Wang, Y. Overview assessment of risk evaluation and treatment technologies for heavy metal pollution of water and soil. *J. Clean. Prod.* **2022**, *379*, 134043. [CrossRef]
89. Tang, Z.; Deng, G.; Hu, G.; Zhang, H.; Pan, H.; Sang, G. Satellite observed spatiotemporal variability of snow cover and snow phenology over High Mountain Asia from 2002 to 2021. *J. Hydrol.* **2022**, *613*, 128438. [CrossRef]
90. Tang, Z.; Wang, X.; Wang, J.; Wang, X.; Li, H.; Jiang, Z. Spatiotemporal Variation of Snow Cover in Tianshan Mountains, Central Asia, Based on Cloud-Free MODIS Fractional Snow Cover Product, 2001–2015. *Remote Sens.* **2017**, *9*, 1045. [CrossRef]
91. Deng, G.; Tang, Z.; Hu, G.; Wang, J.; Sang, G.; Li, J. Spatiotemporal Dynamics of Snowline Altitude and Their Responses to Climate Change in the Tienshan Mountains, Central Asia, during 2001–2019. *Sustainability* **2021**, *13*, 3992. [CrossRef]
92. Wang, S.; Cao, Z.; Luo, P.; Zhu, W. Spatiotemporal Variations and Climatological Trends in Precipitation Indices in Shaanxi Province, China. *Atmosphere* **2022**, *13*, 744. [CrossRef]
93. Zhu, Y.; Luo, P.; Zhang, S.; Sun, B. Spatiotemporal Analysis of Hydrological Variations and Their Impacts on Vegetation in Semiarid Areas from Multiple Satellite Data. *Remote. Sens.* **2020**, *12*, 4177. [CrossRef]
94. Tang, Z.; Ma, J.; Peng, H.; Wang, S.; Wei, J. Spatiotemporal changes of vegetation and their responses to temperature and precipitation in upper Shiyang river basin. *Adv. Space Res.* **2017**, *60*, 969–979. [CrossRef]
95. Zhu, W.; Wang, S.; Luo, P.; Zha, X.; Cao, Z.; Lyu, J.; Zhou, M.; He, B.; Nover, D. A Quantitative Analysis of the Influence of Temperature Change on the Extreme Precipitation. *Atmosphere* **2022**, *13*, 612. [CrossRef]
96. Qin, J.; Duan, W.; Chen, Y.; Dukhovny, V.A.; Sorokin, D.; Li, Y.; Wang, X. Comprehensive evaluation and sustainable development of water-energy-food-ecology systems in Central Asia. *Renew. Sustain. Energy Rev.* **2022**, *157*, 112061. [CrossRef]